

AperTO - Archivio Istituzionale Open Access dell'Università di Torino

**Indocyanine green labeling for optical and photoacoustic imaging of mesenchymal stem cells after in vivo transplantation**

**This is the author's manuscript**

*Original Citation:*

*Availability:*

This version is available <http://hdl.handle.net/2318/1730816> since 2020-02-25T13:56:59Z

*Published version:*

DOI:10.1002/jbio.201800035

*Terms of use:*

Open Access

Anyone can freely access the full text of works made available as "Open Access". Works made available under a Creative Commons license can be used according to the terms and conditions of said license. Use of all other works requires consent of the right holder (author or publisher) if not exempted from copyright protection by the applicable law.

(Article begins on next page)

# Journal of Biophotonics

## Indocyanine Green labeling for optical and photoacoustic imaging of Mesenchymal Stem Cells after in vivo transplantation.

--Manuscript Draft--

<b>Manuscript Number:</b>	
<b>Full Title:</b>	Indocyanine Green labeling for optical and photoacoustic imaging of Mesenchymal Stem Cells after in vivo transplantation.
<b>Article Type:</b>	Full Article
<b>Section/Category:</b>	
<b>Keywords:</b>	Photoacoustic imaging; Cell tracking; Indocyanine Green; stem cells; Near Infrared Fluorescence Imaging.
<b>Corresponding Author:</b>	Miriam Filippi University of Torino Torino, Torino ITALY
<b>Corresponding Author Secondary Information:</b>	
<b>Corresponding Author's Institution:</b>	University of Torino
<b>Corresponding Author's Secondary Institution:</b>	
<b>First Author:</b>	Miriam Filippi
<b>First Author Secondary Information:</b>	
<b>Order of Authors:</b>	Miriam Filippi Francesca Garello Francesca Arena Chiara Pasquino Pierangela Giustetto Federica Antico Enzo Terreno
<b>Order of Authors Secondary Information:</b>	
<b>Abstract:</b>	<p>The transplantation of Mesenchymal Stem Cells (MSCs) holds great promise for the treatment of a plethora of human diseases, but new non-invasive procedures are needed to monitor the cell fate in vivo. Already largely used in medical diagnostics, the fluorescent dye Indocyanine Green (ICG) is an established dye to track limited numbers of cells by optical imaging, but it can be visualized also by Photoacoustic Imaging (PAI), which provides a higher spatial resolution than pure near infrared fluorescence imaging (NIRF). Because of its successful use in clinical and preclinical examinations, we chose ICG as PAI cell labeling agent. Optimal incubation conditions were defined for an efficient and clinically translatable MSC labeling protocol, such that no cytotoxicity or alterations of the phenotypic profile were observed, and a consistent intracellular uptake of the molecule was achieved. Suspensions of ICG-labeled cells were both optically and optoacoustically detected in vitro, revealing a certain variability in the photoacoustic spectra. Intramuscular engraftments of ICG-labeled MSCs were clearly visualized by both PAI and NIRF over few days after transplantation in the hindlimb of healthy mice, suggesting that the proposed technique retains a considerable potential in the field of transplantation-focused research and therapy.</p>
<b>Additional Information:</b>	
<b>Question</b>	<b>Response</b>
Please submit a plain text version of your	January 14th, 2018

cover letter here.

Please note, if you are submitting a revision of your manuscript, there is an opportunity for you to provide your responses to the reviewers later; please do not add them to the cover letter.

Dear Editor,

we are submitting the manuscript entitled 'Indocyanine Green labeling for optical and photoacoustic imaging of Mesenchymal Stem Cells after in vivo transplantation', that reports on the use of the clinically approved fluorescent dye Indocyanine Green (ICG) as labeling agent for the visualization of Mesenchymal Stem Cells (MSCs) by both Photoacoustic and Fluorescence-based Imaging.

The present study was carried out at multiple levels, ranging from the in vitro characterization of the technique to the in vivo applicative proof. Its novelty and significance can be summarised as follows:

- 1)The choice of ICG as a safer alternative to conventional photoacoustic nano-sized probes endows the protocol with maximized safety, thus increasing the potential for clinical translatability. The optimal labeling conditions were determined, by identifying the maximum exposure time to the agent that do not alter the viability, proliferation, and marker profile of cells after incubation.
- 2)In these conditions, a good internalization was obtained, such that efficient optical and photoacoustic imaging of cell suspensions in vitro was feasible, allowing to study the PA spectral properties of ICG.
- 3)Intramuscular engraftments composed of limited numbers ( $3.0 \times 10^5$ ) of labeled MSCs were successfully detected and monitored over time in vivo by both imaging modalities, revealing considerable values of local contrast enhancement in the engraftment site, persisting for days after cell deposition.
- 4)Even though the Fluorescence-based imaging of several types of ICG-labeled cells was already reported (S. E. Boddington, et al., 2010; V. Sabapathy, et al., 2015), our report shows its fundamental role in integrating the photoacoustic information.
- 5)The photoacoustic imaging allowed the video recording of the cell deposition into the tissue during the transplantation, as well as the three-dimensional representation of the engraftments, highlighting the potential utility of the technique in facilitating the collection of data with real-time content and the characterization of the cell engraftments.

Successful preclinical studies fuelled an increasing interest for therapeutic interventions based on the transplantation of stem and progenitor cells, capable of stimulating repair and regeneration of damaged tissue in several diseases affecting the cardiovascular, central nervous, and musculoskeletal system. As the photoacoustic imaging could provide good endogenous contrast among soft tissues and improved spatial resolution with respect to pure optical detection of ICG, in our opinion this efficient, safe and simple labeling technique retains a considerable potential in the field of transplantation-focused research and therapy, possibly being relevant for the future development of new strategies for the cell fate surveillance. As such, we believe this contribution may be of interest to a broader readership.

Yours sincerely,  
Enzo Terreno

# Indocyanine Green labeling for optical and photoacoustic imaging of Mesenchymal Stem Cells after *in vivo* transplantation.

Filippi M.<sup>1#</sup> and Garelo F.<sup>1#</sup>, Arena F.<sup>1</sup>, Pasquino C.<sup>2</sup>, Giustetto P.<sup>1</sup>, Antico F.<sup>2</sup>, Terreno E.<sup>1\*</sup>

<sup>#</sup> These authors contributed equally to this work

<sup>1</sup> Molecular and Preclinical Imaging Centers, Department of Molecular Biotechnology and Health Sciences, University of Turin, Via Nizza 52, 10126 Torino, Italy.

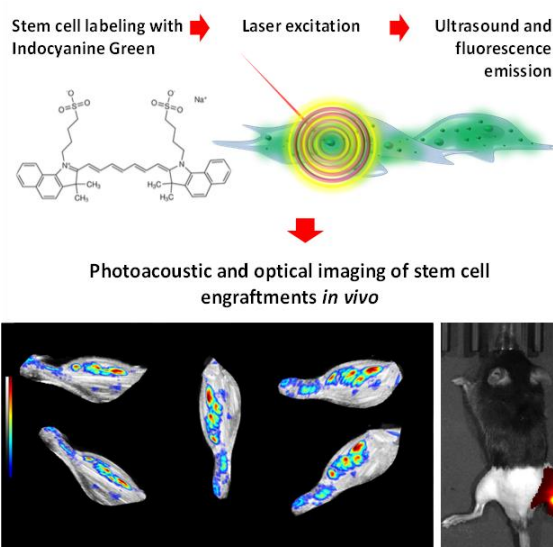
<sup>2</sup> Department of Molecular Biotechnology and Health Sciences, University of Turin, Via Nizza 52, 10126 Torino, Italy.

Received zzz, revised zzz, accepted zzz

Published online zzz

**Key words:** Photoacoustic Imaging; Cell tracking; Indocyanine Green; Stem Cells; Near Infrared Fluorescence Imaging.

The transplantation of Mesenchymal Stem Cells (MSCs) holds great promise for the treatment of a plethora of human diseases, but new non-invasive procedures are needed to monitor the cell fate *in vivo*. Already largely used in medical diagnostics, the fluorescent dye Indocyanine Green (ICG) is an established dye to track limited numbers of cells by optical imaging, but it can be visualized also by Photoacoustic Imaging (PAI), which provides a higher spatial resolution than pure near infrared fluorescence imaging (NIRF). Because of its successful use in clinical and preclinical examinations, we chose ICG as PAI cell labeling agent. Optimal incubation conditions were defined for an efficient and clinically translatable MSC labeling protocol, such that no cytotoxicity or alterations of the phenotypic profile were observed, and a consistent intracellular uptake of the molecule was achieved. Suspensions of ICG-labeled cells were both optically and photoacoustically detected *in vitro*, revealing a certain variability in the photoacoustic spectra acquired by varying the excitation wavelength from 680 to 970 nm. Intramuscular engraftments of ICG-labeled MSCs were clearly visualized by both PAI and NIRF over few days after transplantation in the hindlimb of healthy mice, suggesting that the proposed technique retains a considerable potential in the field of transplantation-focused research and therapy.



Stem cells were labeled with the FDA approved fluorescent dye Indocyanine Green (ICG), and detected by both photoacoustic and optical imaging, enabling to monitor the cell fate safely, in dual modality, and with good sensitivity and improved spatial resolution.

## 1. Introduction

Cell transplantation is an essential tool for biomedical research and a promising approach to achieve curative benefits in several pathologic scenarios.<sup>1</sup> Specifically, due to their major role in regenerative therapies, treatment of immune disorders, and tissue repair, Mesenchymal Stem Cells (MSCs) are commonly involved in cell transplantation-based applications.[1-3] However, these

strategies are not regarded as a first-line therapy yet, mainly because of the limited efficacy shown in several clinical studies.[1,4-5] Since the poor results are very often related to the lack of available information about the cell destiny after transplantation,[4-5] a growing interest has been dedicated to the development of innovative imaging procedures for non-invasive surveillance of the cell fate *in vivo*. [5-6] When the transplantation is performed into superficial tissues, also the imaging techniques with limited penetration depth can be

\* Corresponding author: e-mail: [enzo.terreno@unito.it](mailto:enzo.terreno@unito.it), Phone: +39-0116706452, Fax: +39-0116706478

1  
2 successfully employed to monitor the cell engraftment  
3 and the local biological reaction to the therapy.[7-11]  
4 Both Optical Imaging (OI) and Ultrasonic Imaging (US)  
5 suffer from wave scattering into living tissue, but display  
6 other complementary properties.[12-13] Near Infrared  
7 Fluorescence (NIRF) imaging is one of the most used OI  
8 modalities and it is endowed with elevated sensitivity, but  
9 lacks spatial resolution. On the other side, US imaging  
10 provides a satisfactory sub-mm spatial resolution at  
11 centimeters depth and intermediate sensitivity.[14]  
12 Photoacoustic Imaging (PAI) merges the advantages of  
13 the two techniques and compensates their limitations, thus  
14 paving the way towards new imaging applicative  
15 horizons.[12-13] So far, PA cell imaging has been mostly  
16 performed by loading cells with gold and carbon-based  
17 nano-objects,[15-18] offering a considerable efficiency in  
18 contrast detection, but with documented episodes of  
19 cytotoxicity and adverse immune reactions.[16,19-20]  
20 However, also small molecules (either fluorescence  
21 quenchers or low quantum-yield emitters) display  
22 properties of interaction with the electromagnetic  
23 radiation leading to photothermal conversion and ultrasonic  
24 emission.[21] Among fluorescent compounds, we chose  
25 Indocyanine Green dye (ICG), a tricyanocyanine dye that,  
26 when dissolved in aqueous solution in the micromolar  
27 range, exhibits absorbance and emission peaks at 780 nm  
28 and 830 nm, respectively.[22-23] Since its FDA approval  
29 for human use in 1959,[22] this molecule has been  
30 clinically employed for a myriad of medical purposes,  
31 including phototherapy, ophthalmic angiography,  
32 laparoscopy, hepatic function and cardiac output  
33 determination, sentinel lymph node detection in oncology,  
34 vascular and brain surgery, and several others.[22-27]  
35 With a fluorescence quantum yield of about 10% in water,  
36 ICG can non-radiatively release  $\approx 90\%$  of its excited  
37 energy in the form of heat,[28] thus becoming a popular  
38 option for the surface functionalization of particles  
39 detectable by both NIRF and PAI.[15,21] ICG has already  
40 been proposed as cell labeling agent in cell tracking by  
41 NIRF,[29-30] but it has never been envisaged for the  
42 photoacoustic cell visualization in its molecular form.  
43 Besides retaining superior imaging potential than pure  
44 NIRF, PAI of cells loaded with ICG would also offer a  
45 safer labeling route than current standard probes.  
46 Therefore, in the present study, this dye was selected as  
47 dual fluorescence and optoacoustic cell tracer to label  
48 murine bone marrow-derived MSCs. After having defined  
49 the optimal labeling conditions, the characteristics and  
50 persistence of NIRF and PA signals were monitored either  
51 in *in vitro* cell suspensions or *in vivo* engraftments  
52 obtained by intramuscular transplantation in healthy mice.  
53

## 54 2. Experimental

### 55 2.1 Animal Care and Use

56  
57  
58  
59  
60  
61  
62  
63  
64  
65  
66  
67  
68  
69  
70  
71  
72  
73  
74  
75  
76  
77  
78  
79  
80  
81  
82  
83  
84  
85  
86  
87  
88  
89  
90  
91  
92  
93  
94  
95  
96  
97  
98  
99  
100  
101  
102  
103  
104  
105  
106  
107  
108  
109  
110  
111  
112  
113  
114  
115  
116  
117  
118  
119  
120  
121  
122  
123  
124  
125  
126  
127  
128  
129  
130  
131  
132  
133  
134  
135  
136  
137  
138  
139  
140  
141  
142  
143  
144  
145  
146  
147  
148  
149  
150  
151  
152  
153  
154  
155  
156  
157  
158  
159  
160  
161  
162  
163  
164  
165  
166  
167  
168  
169  
170  
171  
172  
173  
174  
175  
176  
177  
178  
179  
180  
181  
182  
183  
184  
185  
186  
187  
188  
189  
190  
191  
192  
193  
194  
195  
196  
197  
198  
199  
200  
201  
202  
203  
204  
205  
206  
207  
208  
209  
210  
211  
212  
213  
214  
215  
216  
217  
218  
219  
220  
221  
222  
223  
224  
225  
226  
227  
228  
229  
230  
231  
232  
233  
234  
235  
236  
237  
238  
239  
240  
241  
242  
243  
244  
245  
246  
247  
248  
249  
250  
251  
252  
253  
254  
255  
256  
257  
258  
259  
260  
261  
262  
263  
264  
265  
266  
267  
268  
269  
270  
271  
272  
273  
274  
275  
276  
277  
278  
279  
280  
281  
282  
283  
284  
285  
286  
287  
288  
289  
290  
291  
292  
293  
294  
295  
296  
297  
298  
299  
300  
301  
302  
303  
304  
305  
306  
307  
308  
309  
310  
311  
312  
313  
314  
315  
316  
317  
318  
319  
320  
321  
322  
323  
324  
325  
326  
327  
328  
329  
330  
331  
332  
333  
334  
335  
336  
337  
338  
339  
340  
341  
342  
343  
344  
345  
346  
347  
348  
349  
350  
351  
352  
353  
354  
355  
356  
357  
358  
359  
360  
361  
362  
363  
364  
365  
366  
367  
368  
369  
370  
371  
372  
373  
374  
375  
376  
377  
378  
379  
380  
381  
382  
383  
384  
385  
386  
387  
388  
389  
390  
391  
392  
393  
394  
395  
396  
397  
398  
399  
400  
401  
402  
403  
404  
405  
406  
407  
408  
409  
410  
411  
412  
413  
414  
415  
416  
417  
418  
419  
420  
421  
422  
423  
424  
425  
426  
427  
428  
429  
430  
431  
432  
433  
434  
435  
436  
437  
438  
439  
440  
441  
442  
443  
444  
445  
446  
447  
448  
449  
450  
451  
452  
453  
454  
455  
456  
457  
458  
459  
460  
461  
462  
463  
464  
465  
466  
467  
468  
469  
470  
471  
472  
473  
474  
475  
476  
477  
478  
479  
480  
481  
482  
483  
484  
485  
486  
487  
488  
489  
490  
491  
492  
493  
494  
495  
496  
497  
498  
499  
500  
501  
502  
503  
504  
505  
506  
507  
508  
509  
510  
511  
512  
513  
514  
515  
516  
517  
518  
519  
520  
521  
522  
523  
524  
525  
526  
527  
528  
529  
530  
531  
532  
533  
534  
535  
536  
537  
538  
539  
540  
541  
542  
543  
544  
545  
546  
547  
548  
549  
550  
551  
552  
553  
554  
555  
556  
557  
558  
559  
560  
561  
562  
563  
564  
565  
566  
567  
568  
569  
570  
571  
572  
573  
574  
575  
576  
577  
578  
579  
580  
581  
582  
583  
584  
585  
586  
587  
588  
589  
590  
591  
592  
593  
594  
595  
596  
597  
598  
599  
600  
601  
602  
603  
604  
605  
606  
607  
608  
609  
610  
611  
612  
613  
614  
615  
616  
617  
618  
619  
620  
621  
622  
623  
624  
625  
626  
627  
628  
629  
630  
631  
632  
633  
634  
635  
636  
637  
638  
639  
640  
641  
642  
643  
644  
645  
646  
647  
648  
649  
650  
651  
652  
653  
654  
655  
656  
657  
658  
659  
660  
661  
662  
663  
664  
665  
666  
667  
668  
669  
670  
671  
672  
673  
674  
675  
676  
677  
678  
679  
680  
681  
682  
683  
684  
685  
686  
687  
688  
689  
690  
691  
692  
693  
694  
695  
696  
697  
698  
699  
700  
701  
702  
703  
704  
705  
706  
707  
708  
709  
710  
711  
712  
713  
714  
715  
716  
717  
718  
719  
720  
721  
722  
723  
724  
725  
726  
727  
728  
729  
730  
731  
732  
733  
734  
735  
736  
737  
738  
739  
740  
741  
742  
743  
744  
745  
746  
747  
748  
749  
750  
751  
752  
753  
754  
755  
756  
757  
758  
759  
760  
761  
762  
763  
764  
765  
766  
767  
768  
769  
770  
771  
772  
773  
774  
775  
776  
777  
778  
779  
780  
781  
782  
783  
784  
785  
786  
787  
788  
789  
790  
791  
792  
793  
794  
795  
796  
797  
798  
799  
800  
801  
802  
803  
804  
805  
806  
807  
808  
809  
810  
811  
812  
813  
814  
815  
816  
817  
818  
819  
820  
821  
822  
823  
824  
825  
826  
827  
828  
829  
830  
831  
832  
833  
834  
835  
836  
837  
838  
839  
840  
841  
842  
843  
844  
845  
846  
847  
848  
849  
850  
851  
852  
853  
854  
855  
856  
857  
858  
859  
860  
861  
862  
863  
864  
865  
866  
867  
868  
869  
870  
871  
872  
873  
874  
875  
876  
877  
878  
879  
880  
881  
882  
883  
884  
885  
886  
887  
888  
889  
890  
891  
892  
893  
894  
895  
896  
897  
898  
899  
900  
901  
902  
903  
904  
905  
906  
907  
908  
909  
910  
911  
912  
913  
914  
915  
916  
917  
918  
919  
920  
921  
922  
923  
924  
925  
926  
927  
928  
929  
930  
931  
932  
933  
934  
935  
936  
937  
938  
939  
940  
941  
942  
943  
944  
945  
946  
947  
948  
949  
950  
951  
952  
953  
954  
955  
956  
957  
958  
959  
960  
961  
962  
963  
964  
965  
966  
967  
968  
969  
970  
971  
972  
973  
974  
975  
976  
977  
978  
979  
980  
981  
982  
983  
984  
985  
986  
987  
988  
989  
990  
991  
992  
993  
994  
995  
996  
997  
998  
999  
1000

### 2.2 Chemicals

All the materials necessary for cell culture were purchased from Lonza (Lonza Sales AG, Verviers, Belgium). The ICG dye was purchased from MP Biomedicals (Santa Ana, CA, USA), whereas all other chemicals from Sigma Chemical Co. (St Louis, MO, USA) and were used as received.

### 2.3 MSC culture

MSCs were isolated from the bone marrow of male C57BL/6J mice (age: 7-9 weeks, weight: 22-28 g). Briefly, femurs and tibias were excised, and flushed with RPMI w/o Red Phenol supplemented with 10% FBS to harvest the bone marrow cells, which were then cultured into Minimal Essential Medium Eagle Alpha Modification supplemented with penicillin (100 U/ml), streptomycin (100  $\mu\text{g}/\text{ml}$ ), FBS (10%) and glutamine (2 mM). After 4 days, the MSCs were selected on the basis of their adherence to plastic, before they underwent a magnetic immune cell sorting with Microbeads conjugated to monoclonal rat antimouse/human CD11b antibody (Miltenyi Biotec GmbH, Bergish Gladbach, Germany) at day 10 to further remove CD11b<sup>+</sup> granulocytic cells.

### 2.4 Cell labeling protocol

The ICG-labeling solution was prepared by completely dissolving the dye powder into Dimethyl Sulfoxide (DMSO), before adding the FBS-free culture medium (the v/v of DMSO/medium was 1:6). A final ICG concentration of 0.25 mg/ml was used in all experiments. MSCs were detached from flasks, added with the pre-warmed ICG-labeling solution, and left at 37°C for variable time ranges (ranging from 2 minutes to 6 hours). After labeling, the excess of dye was removed by washing the cells three times with Phosphate Buffered Saline (PBS).

### 2.5 Cell viability and proliferation rate

Cell viability was estimated by using the Trypan Blue exclusion assay. The reported viability percentage value represents the average ratio between the number of viable

1  
2 cells  $N_v$  and the total number of cells  $N_{tot}$  ( $N_v/N_{tot} \times 100$ ).  
3 Similarly, for proliferation tests the cells were seeded after  
4 labeling and maintained in standard culture conditions for  
5 different time ranges (up to 8 days), before being counted.  
6 The proliferation ability is expressed as the average ratio  
7 between the number of cells at each time point  $N_t$  and the  
8 number of cells present at the beginning of the experiment  
9  $N_0$  ( $N_t/N_0$ ).

## 10 2.6 Flow cytometry

11 Cells were resuspended in PBS supplemented with 0.1%  
12 BSA and incubated with fluorochrome-conjugated  
13 monoclonal antibodies (mAb) for 30 min at 4°C. The  
14 following mAbs (final dilution: 1/20) were used: anti-  
15 CD29-(PE), anti-CD44-APC, anti-CD11b-FITC, anti-  
16 CD90-(PE) (BD Bioscience Pharmingen, San Jose, CA,  
17 USA), anti-Sca1-(PE) (Cedarlane, Burlington, Ontario,  
18 Canada), and anti-CD105-PE (MACS Miltenyi Biotec,  
19 San Diego, CA, USA). The fluorescence was measured  
20 using the FACS Calibur flow cytometer equipped with  
21 CellQuest software (BD Biosciences).

## 22 2.7 Optical absorbance and emission of labeled 23 cells

24 The cell uptake of ICG was estimated by fluorimetry.  
25 Briefly, the labeling incubation was carried on for 60  
26 minutes. After exhaustive washing, cells were counted,  
27 suspended at the final concentration of  $3.0 \times 10^6$  cells/ml in  
28 PBS, sonicated by using a Bandelin Sonoplus Sonicator  
29 (20kHz, 20 W, 30s), and analysed by a FluoroMax-4  
30 Spectrofluorometer (Horiba Scientific, Edison New  
31 Jersey, USA) equipped with the driving software  
32 FluorEssence™ for Windows. The number of ICG  
33 molecules internalized by the single cell was estimated on  
34 the basis of the signal intensity values measured at 803 nm  
35 and reported on the calibration curves which were  
36 previously obtained. The experiment was repeated four  
37 times.

## 38 2.8 Cell transplantation

39 Healthy male C57BL/6J mice (weight: 25-28 g, age: 10-  
40 12 weeks) were anaesthetized, and their hindlimbs were  
41 shaved. After labeling,  $3.0 \times 10^5$  MSCs were collected,  
42 suspended in 100  $\mu$ L of PBS, and injected into the  
43 gastrocnemius muscle of the right hindlimb by using a 1-  
44 ml syringe with a 25-G  $\times$  5/8-in needle (BD, Franklin  
45 Lakes, NJ). Equivalent numbers of control unlabeled cells  
46 were transplanted into the left hindlimb.

## 47 2.9 Combined ultrasound and photoacoustic 48 (US/PA) imaging

49 PAI was performed by using a VisualSonics Vevo 2100  
50 LAZR Imaging Station (VisualSonics, Inc., Toronto,  
51 Canada) equipped with a LZ250 transducer operating at  
52 21 MHz frequency that incorporates photoacoustic  
53 imaging into high-resolution ultrasound imaging. Cell  
54 suspensions were loaded onto a custom-made phantom for

photoacoustic *in vitro* acquisitions, equipped with  
stretched plastic capillaries to contain liquid samples,  
further surrounded by solidified agarose gel to provide  
favourable interface for US propagation. The  
photoacoustic transducer was set perpendicularly to the  
capillaries, such that images reproducing their axial  
sections were acquired. The PA signal intensity was  
recorded by switching the excitation over the wavelength  
range included between 680 and 960 nm, and graphed as  
a spectrum. The normalized photoacoustic spectrum for  
each sample was obtained by subtracting the contribution  
of the blank (either PBS or unlabeled cells suspended in  
PBS) at each wavelength  $\lambda$ , as follows:

$$NPA_{\lambda} = PA_{sample \lambda} - PA_{ctrl \lambda}$$

where  $NPA$  is the normalized photoacoustic signal,  
 $PA_{sample}$  and  $PA_{ctrl}$  stand for the photoacoustic intensity  
at each wavelength  $\lambda$  of each *sample* or *ctrl*, respectively.  
Each experiment was repeated in triplicate.

For *in vivo* imaging, anaesthetized animals were  
accurately shaved on their hindlimbs. Combined US/PA  
images were obtained by overlaying photoacoustic  
intensities on the ultrasound images with user-defined  
grayscale thresholds. PA intensity values measured on the  
transplantation site of labeled cells (right hindlimb) were  
normalized with respect to the signal recorded on the same  
anatomical region of the left hindlimb after the injection  
of the control unlabeled cells, as reported in the following  
formula:

$$PA_{Enh} = \frac{PA_{right} - PA_{left}}{PA_{left}}$$

where  $PA_{right}$  and  $PA_{left}$  represent the photoacoustic  
signal measured in the right and left hindlimb at different  
wavelengths included between 680 and 960 nm,  
respectively. Spectra recorded before the cell  
transplantation (Pre-Injection) were provided to show the  
local endogenous photoacoustic baseline of the muscular  
tissue. The signal intensity quantification was carried out  
at fixed excitation wavelength (810 nm).

## 51 2.10 Optical imaging

52 The photon emission from the labeled cells was measured  
53 *in vitro* on the Pearl Imager (LI-COR Biosciences,  
54 Lincoln, NE) with preset near infrared excitation (710-  
55 760 nm) and emission (810-875 nm) pass band filters to  
56 evaluate the ICG signal. The *in vivo* studies were carried  
57 out on the IVIS Spectrum Whole Animal Imaging System  
58 (Perkin Elmer Inc., Waltham, Massachusetts, USA). The  
59 animals were irradiated with filter light of wavelength 745  
60 nm, and an image of emission intensity was collected at  
61 840 nm (field of view = 14 cm, fstop = 2, binning =  
62 medium, exposure time = auto). As for the photoacoustic  
63 experiments, the fluorescence-imaging signal intensity  
64 values were measured on the transplantation site of  
65 labeled cells (right hindlimb), and normalized with respect

1  
2 to control unlabeled cells (left hindlimb). The  
3 Fluorescence Imaging Enhancement ( $FLEnh$ ) was  
4 expressed as:

$$5 \quad FLEnh = \frac{FLE_{right} - FLE_{left}}{FLE_{left}}$$

6  
7  
8 where  $FLE_{right}$  and  $FLE_{left}$  represent the fluorescence  
9 intensity measured in the right and left hindlimb,  
10 respectively.

### 11 12 13 2.11 Statistical analysis

14 All data were presented as Mean Values  $\pm$  Standard Error  
15 of the Mean (MV $\pm$ SE). Statistical significance was  
16 determined by either the unpaired Student *t*-test or the  
17 Analysis of the Variance (ANOVA) test, as indicated in  
18 each graph. The *p*-values  $\leq 0.05$  and  $0.01$  were marked as  
19 \* and \*\*, respectively.  
20  
21

## 22 23 3. Results

### 24 25 3.1 Optimization of the cell labeling procedure

26 The labeling procedure was performed by detaching and  
27 incubating MSCs with ICG-containing medium at 37°C  
28 (**Figure 1A**). According to previous studies,[31] a final  
29 ICG concentration of 0.25 mg/mL was selected to perform  
30 all labeling experiments, and the procedure was optimized  
31 by subjecting the MSCs to different incubation times. For  
32 the longest incubation times, an inverse proportionality  
33 between cell viability and duration of the labeling was  
34 observed (**Figure 1B**), with a significant (*t*-test *p*-value  $\leq$   
35 0.01) viability reduction specifically induced by  
36 incubations lasting 3 and 6 h (18.9% and 24.3%,  
37 respectively). In these conditions, cells also showed  
38 impaired proliferation ability (**Figure 1C**): a decreased  
39 fraction of viable cells was found at different time points  
40 after labeling, culminating at day 8 when the proliferation  
41 rate for both the conditions was dramatically reduced  
42 (33.3 % and 40.7 %, respectively, ANOVA *p*-value  $\leq$   
43 0.01) with respect to control cells. In the other tested  
44 labeling times, no relevant changes in viability were  
45 detected, therefore suggesting that an incubation time of 1  
46 h may be considered optimal for safe labeling in  
47 maximum loading conditions. The molecular  
48 internalization rate after 1h incubation was therefore  
49 determined by estimating the ICG content per cell via  
50 fluorimetric assay directly on labeled cell suspensions,  
51 such that an uptake of  $(1.7 \pm 0.4) \times 10^{10}$  molecules/cell was  
52 calculated, corresponding to an internalization efficiency  
53 of approximately  $0.9 \pm 0.2$  %. Finally, as observed by flow  
54 cytometry, the 1 h exposure to ICG did not induce any  
55 alteration in the expression profile of cell surface markers  
56  
57  
58  
59

(**Figure 1D**), revealing a complete retention of the MSC  
phenotype.

### 3.2 In vitro imaging

The photoacoustic and fluorescent properties of ICG were  
preliminary investigated with the respective imaging  
systems (**Figure 2 and 3**). The photoacoustic signal of  
differently concentrated ICG aqueous solutions in a  
submillimolar range was acquired by tuning the excitation  
wavelength from 680 to 970 nm in order to study the PA  
sensitivity and spectrum *in vitro* (**Figure 2A and B**). The  
intensity at the initial phase of the spectral profile  
increased with the dye concentration, and even if a  
photoacoustic detection limit of 25  $\mu$ M was identified  
elsewhere on a different PA imaging station,[32] in our  
setup we were able to clearly detect the molecule at a  
concentration of 15  $\mu$ M (**Figure 2A**) according to what  
was already reported by others using the same  
instrument.[33] The PA signal tended to drop as the  
excitation was swept to high wavelengths ( $> 830$  nm) and  
became eventually negligible at 950 nm, even at the  
highest concentration tested (*i.e.*, 1 mM). However, a  
certain concentration-dependent variability in the spectral  
shapes was observed: whereas the 1 mM ICG presented a  
sharp peak centered at 710 nm, in diluted solutions the  
molecule displayed a more flattened spectral profile  
characterized by the presence of two peaks. Further  
lowering the concentration, a more defined peak at 800  
nm appeared. Since this observation approximately  
matched the finding of a recurrent main peak at around  
810 nm reported by Park *et al.*[32], we selected this  
excitation wavelength as reference value to perform the  
signal quantification and acquire representative images. In  
order to test the effects of a possible interaction between  
ICG and cellular components, samples containing the dye  
at variable concentrations and a fixed number ( $3.0 \times 10^5$ ) of  
MSCs were analyzed immediately after mixing (**Figure**  
**2C and D**). Interestingly, in the presence of cells the PA  
signal intensity at the spectral initial phase increased for  
almost all the samples (*ca.* 2-fold increase at 15 and 100  
 $\mu$ M and even 3-fold at 1 mM ICG). Although some  
variations in the spectral shape were observed at the  
highest investigated ICG concentration, for the  
micromolar ICG the main peak wavelength shifted within  
the 800-820 nm interval, confirming that the PA  
excitation may be performed at maximum efficacy in this  
range. Finally, also cells labeled with the ICG according  
to our optimized protocol were analyzed (**Figures 2E and**  
**2F**). This experiment was carried out by resuspending  
 $3.0 \times 10^5$  ICG-labeled MSCs in decreasing PBS volumes,  
thus varying both the cell density and the final volume of  
the suspension. We assumed that the ICG amount uptaken  
by the cells during the labeling procedure led to a final dye

1  
2 concentration in the  $\mu\text{M}$  range, as it was previously  
3 determined by fluorimetry. Indeed, the spectral shape of  
4 the labeled MSCs recapitulated the one observed in the  
5 presence of the micromolar dye, being characterized by a  
6 main peak at about 820 nm. Very interestingly, the ICG  
7 internalized within cells produced a strong PA signal,  
8 which increased of *ca.* 25 % and 85 % as compared to the  
9 100  $\mu\text{M}$  ICG sample with and without cells, respectively.  
10 Indeed, the PA signal intensity was comparable to that of  
11 the 1 mM ICG mixed with cells (**Figure 2G**), thus  
12 indicating that an optoacoustic enhancement can likely be  
13 obtained through the intracellular compartmentalization  
14 of the dye. Interestingly, only subtle variations in the PA  
15 signal intensity were found when labeled cells were  
16 differently concentrated into PBS (**Figures 2E and 2F**),  
17 possibly suggesting that phenomena of liquid reabsorption  
18 that commonly follow the inoculation of cells into tissue  
19 might only induce minimal effects on the signal intensity.  
20 All the samples were also analyzed in terms of NIRF  
21 intensity, as expressed in Average Radiant Efficiency  
22 (**Figure 3**). For both ICG aqueous solutions and ICG-cell  
23 mix, the concentration-dependent initial increase of the  
24 fluorescence peaked at 50  $\mu\text{M}$ , and was followed by a fast  
25 decrease (**Figures 3A and 3B**) in accordance to previous  
26 studies indicating that dye concentrations exceeding 200  
27  $\mu\text{M}$  are not detectable due to quenching phenomena.[32]  
28 The fluorescent behaviour of ICG only differed at 100  
29  $\mu\text{M}$ , where a slightly reduced emission occurred in the  
30 presence of cells. Interestingly, in the suspensions of ICG-  
31 labeled cells (**Figures 3C and 3D**) the NIRF contrast  
32 enhancement calculated over the baseline (unlabelled  
33 cells) at the lowest and highest cell concentrations  
34 (namely 3000 and 15000 cell/ $\mu\text{l}$ ) corresponded to +300  
35 and 220%, respectively, therefore showing a mild  
36 reduction of the fluorescent emission towards high cell  
37 densities. Nonetheless, these signal variations were  
38 recorded in the same magnitude range of intensity,  
39 reflecting a relatively limited potential of the cell density  
40 to affect the NIRF emission. Additionally, we also  
41 demonstrated that both the photoacoustic and fluorescent  
42 emissions increased with the incubation time (**Figure**  
43 **S1A**), but whereas the PA signal amplitudes recorded on  
44 suspensions of cells labeled for 2 minutes were not  
45 distinguishable from the baseline, the fluorescent signal  
46 could be detected in all the tested conditions (**Figure**  
47 **S1B and C**). Finally, the PA and NIRF signal intensity from  
48 cells incubated for 1 h was significantly (ANOVA, *p*-  
49 value < 0.01) higher with respect to all other conditions  
50 (**Figures S1A and S1B**), confirming this incubation time  
51 as optimal for imaging efficiency.

### 52 3.3 *In vivo* imaging

The *in vivo* study was carried out by locally transplanting  
3.0 $\times 10^5$  ICG-labeled MSCs into the gastrocnemius  
muscle of the right hindlimb of healthy C57BL/6J mice.  
The site of cell deposition was clearly detected by US  
imaging (B-mode, 21 MHz), as a consequence of the  
change in the acoustic impedance determined by the dense  
inoculated cell mass (**Figure 4A**). The PA signal intensity  
generated by the ICG-MSCs was normalized over the  
local endogenous baseline recorded in the left hindlimb of  
the animal where the transplantation of control unlabeled  
cells was performed (representative pictures in **Figure**  
4**B**) and expressed as photoacoustic enhancement ( $PA_{Enh}$ ,  
see Experimental for details). The  $PA_{Enh}$  was measured  
over the entire range of excitation wavelengths  
immediately after cell transplantation, then monitored  
over time, and reported as PA spectrum in **Figure 4C**.  
Interestingly, immediately and 4 hours post-injection, the  
maximum peak recorded in the photoacoustic spectra was  
shifted towards high excitation wavelength values (890  
and 920 nm, respectively), whereas from day 1 to day 4,  
the spectral shape reproduced the one observed *in vitro*  
with a maximum enhancement centered at around 810 nm  
(**Figures 4D and 4E**). Finally, the normalized PA spectra  
acquired 7 days post injection presented a flat shape  
without any discernable peak. **Figure 4F** displays the  
time-dependent variation of the signal as quantified at  
both 810 nm and the wavelength corresponding to the  
maximum peak recorded in each spectrum, whereas  
**Figure 4G** shows representative images of the time  
evolution of PA emission in regions of interest (ROIs) at  
tissue depth comprised between 1 and 5 mm. Moreover,  
the entire procedure of cell injection was caught on video  
(**Movie S1**) and 3D reconstructions of the ICG-MSC  
engraftment in the right calf were elaborated using  
Vevo@Lab 1.7.2 software (**Figure S2 and Movies S2 and**  
5**S3**). Immediately after cell transplantation, a considerably  
high PA amplitude was measured in the inoculation site  
(**Figures 4C and 4F**). By summing up the PA signal areas  
as calculated on bidimensional ROIs drawn in consecutive  
images over the entire muscular region, an engraftment  
volume of around 70  $\text{mm}^3$  was estimated, which is  
consistent to the injection procedure of a 100  $\mu\text{l}$  cell  
suspension. Then, a progressive time-dependent decrease  
in the signal intensity occurred, revealing that the labeled  
MSCs could be optoacoustically detected until 3 days  
before the loss of the ICG-related signal and the  
prevalence of unspecific signal components let the  
contrast enhancement become almost negligible (**Figure**  
4**F**). After each PA acquisition, the mice underwent NIRF  
imaging in order to assess the fluorescent contrast  
enhancement ( $FLI_{Enh}$ ) produced by the transplanted cells  
(**Figures 5A and 5B**). Interestingly, before progressively  
fading over days (likely due to the dye degradation and  
washout), the  $FLI_{Enh}$  values followed an initial rising trend  
during the first 24 h after the engraftment deposition. The  
coincident observation of extremely high PA amplitudes  
(**Figures 4C and 4F**) suggests that at early time points the  
strong intermolecular interactions among ICG molecules



1  
2 contribute to the quenching of the fluorescence, but  
3 results at the same time into an increase of the  
4 photoacoustic effect, due to photothermal conversion by  
5 nonradiative decay.[33] Finally, the time limit for the  
6 engraftment detection by NIRF matched that one enabled  
7 by the photoacoustic decay (namely, 3 days *p.i.*). Similar  
8 conclusions derived from an additional series of  
9 experiments performed by transplanting a higher cell  
10 number ( $1.0 \times 10^6$  cells, **Figures S3 and S4**). As expected,  
11 a more intense and persistent contrast enhancement was  
12 obtained in both techniques, pushing further the detection  
13 limit day. In particular, a photoacoustic signal was still  
14 detected 7 days after transplantation, which truly  
15 corresponded to sparse residual ICG-labeled MSCs, as  
16 proved by histological examination in the inoculation site  
17 (**Figure S5**).

#### 20 4. Discussion

21  
22  
23 According to pre-clinical and clinical research conducted  
24 thus far, cell imaging should be assimilated into more  
25 studies focused on the use of cell-transplantation for  
26 therapeutic purposes.[30] In fact, the imaging techniques  
27 that facilitate the unambiguous *in vivo* identification and  
28 characterization of the cell engraftments are invaluable for  
29 assessing the survival and the functional integration of  
30 exogenous cells, and for optimizing the delivery as well.  
31 The present work aimed at addressing these issues by  
32 merging the advantages offered by the well-known and  
33 safe profile of ICG with the emergent technique of PAI.  
34 For the first time the potential application of the free ICG  
35 as cell labeling agent and photoacoustic tracer was  
36 explored. As already done by Uthaman *et al.*,[34] the PA  
37 visualization of the cell engraftment was paralleled by  
38 NIRF acquisition in order to perform a comparative study  
39 of the two imaging modalities. Despite the minor toxicity  
40 and the related advantages for *in vivo* applications, ICG  
41 exhibits very complex optical properties. Besides being  
42 largely dependent on the solvent, concentration and  
43 interaction with other molecules,[22,23,26] the absorption  
44 and emission spectra are also broad and overlapping, thus  
45 causing a significant re-absorption of the fluorescence by  
46 the dye itself. Moreover, as extensively reviewed by  
47 Desmettre *et al.*,[22] the molecule can be affected by  
48 photodegradation and, at high concentrations, its effective  
49 absorption does not linearly increase with concentration  
50 due to the dye aggregation. More in details, because of its  
51 amphiphilic properties, ICG is mainly present in the  
52 monomer form at concentrations below 5  $\mu\text{M}$ , whereas  
53 over 100  $\mu\text{M}$  the oligomer form prevails. The ICG  
54 oligomers display a weaker fluorescence yield, affecting  
55 the absorbance spectrum. Thus, a dramatic boost of the  
56 ICG concentration is not expected to result in a substantial  
57 signal enhancement, as we also noticed by both PA and  
58 NIRF imaging. Alternatively, in order to increase the  
59 quantum yield and the fluorescence intensity of the

carbocyanine dye, a stable interaction with phospholipids  
could be envisaged.[35] Such crucial aspect has been  
extensively exploited for the preparation of several ICG-  
loaded nanosystems thus far,[35-36] and coherently, in  
our experiments the simple mixture of ICG with cells  
produced a marked increase in the PA intensity values,  
which could be possibly ascribed also to its interaction  
with cell membranes. On the other hand, the additional PA  
increase we observed in the cells after incubation with the  
dye could be hypothetically justified also by a mechanism  
of oligomer formation occurring as a consequence of the  
intracellular compartmentalization. Importantly, in the  
present study a cell labeling procedure advantageous in  
terms of both cellular uptake and generated imaging signal  
was proposed. Remarkably, in these conditions the  
exposure to the contrast agent did not produce any  
relevant alteration in the cell profile, suggesting that ICG-  
labeled MSCs may retain their therapeutic efficacy.  
Finally, when it comes to *in vivo* use of the ICG, the  
results interpretation is further complicated by the  
intricacy of molecular interactions with the various  
components of the biological environment.[22,34] Here,  
the photoacoustic behaviour of the dye was investigated  
in complex circumstances involving concentration-  
dependent effects, internalization by cells, interactions  
with cell components, and deposition into living tissues.  
Since several common applicative scenarios require the  
transplantation of hundreds of thousands of MSCs,[37-38]  
we representatively performed our experiments by  
labeling and monitoring  $3.0 \times 10^5$  cells to verify whether  
this procedure could be of effective utility and practical  
interest. Our *in vivo* proof of principle productively  
demonstrated that cells can be visualized into living tissue  
by both PAI and NIRF over few days after transplantation.  
Though the ICG labeling enables the longitudinal  
monitoring of the engrafted cells, the observation times  
are shorter than for the PA-detectable nano-objects  
reported in literature,[17] most likely due to the faster  
release of the dye from cells, as already observed by  
Boddington *et al.*[29] However, also the risks connected  
to the long-term tissue accumulation of exogenous  
compounds have to be carefully considered, especially in  
proximity of delicate therapeutic cell grafts. Additionally,  
we established that a reliable quantification of the  
photoacoustic signal at 810 nm can be performed only  
starting from 24 h after transplantation, since the prior  
time points are affected by a bathochromic shift of the  
ICG signal, possibly related to the extremely high local  
concentration of the dye. As in the same time window we  
detected the co-presence of PA peaks centred at around  
900 nm and reduced NIRF signal, we argued that the two  
phenomena may be correlated by an exchange of the  
emission mechanism (*i.e.* from radiative to acoustic),  
likely depending on the ICG concentration. However, in  
general terms, it also has to be taken into account that  
immediately or shortly after surgery, tissues frequently  
display imaging artefacts caused by haemorrhages and/or  
micro air bubbles deposition, which make it arduous to

1  
2 define the real source of the observed contrast, thus  
3 preventing an accurate quantification in early monitoring.  
4 This aspect becomes more relevant when the local  
5 transplantation is carried out in the absence of specific cell  
6 vehicles (like hydrogels), such that the injection procedure  
7 likely introduces air into tissue along the needle path.[39]  
8 Therefore, we conclude that the optimal imaging window  
9 offered by the present protocol corresponds to a time  
10 range comprised between 1 and 3 days post-  
11 transplantation, which could ideally turn out to be helpful  
12 in prospective clinical or pre-clinical applications to: (i)  
13 ascertain the successful outcome of surgical cell  
14 deposition, (ii) describe the extension and aspect of the  
15 engraftment, and (iii) follow the cell migration in  
16 relatively superficial anatomical areas. Finally, we  
17 demonstrated that NIRF imaging substantially  
18 recapitulated and validated the information obtained by  
19 PAI, thus highlighting the pivotal role of the dual-  
20 modality approach in strengthening the reliability and  
21 clinical utility of ICG-guided MSC imaging. In the past  
22 decade, researchers have been tracking transplanted cells  
23 in real-time *in vivo* mainly by Magnetic Resonance  
24 Imaging (MRI), Positron emission Tomography (PET),  
25 Single Photon Emission Tomography (SPECT), and  
26 Optical Imaging, facing crucial issues in regard to image  
27 acquisition time, method sensitivity, radiation-related  
28 damage, short half-life of radioisotopes, genetic  
29 manipulation to introduce reporter genes, and three  
30 dimensional anatomical imaging capability.[5-11,39] The  
31 high spatial resolution integrated with elevated sensitivity  
32 and moderate tissue penetration depth, the FDA-approved  
33 tracer and the fast image acquisition make of the herein  
34 proposed protocol an attractive option to further develop  
35 the techniques of direct stem cell labeling towards the  
36 clinical dimension, by satisfying almost all the ideal  
37 translational requirements.[40]

## 5. Conclusion

38  
39  
40  
41  
42 In summary, the ICG was successfully used as PA-NIRF  
43 dual-mode contrast agent to label, visualize, and monitor  
44 MSCs both *in vitro* and *in vivo*. Proper cell labeling  
45 conditions were selected such that the cell uptake was  
46 maximized, and cell viability, proliferation, and  
47 phenotypic features were preserved. Since the number of  
48 MSCs involved in several experimental circumstances is  
49 usually either similar or higher than that used here,[35-36]  
50 we conclude that in a forward-looking vision this  
51 technique retains a considerable potential for  
52 transplantation-focused research and therapy by providing  
53 the *in vivo* cell fate surveillance with safety, real time  
54 content, good endogenous contrast among soft tissues and  
55 improved spatial resolution.  
56  
57  
58  
59

## Supporting Information

Additional supporting information may be found in the  
online version of this article at the publisher's website.

**Acknowledgements** Dr Giovanni Valbusa (Ephoran),  
Lorenzo Ariotti (Bracco Imaging Spa), and Dr Marta Tapparo  
(University of Turin) are gratefully acknowledged for their  
valuable contribution to fluorescence microscopy imaging and  
histological examination. FUV is gratefully acknowledged.

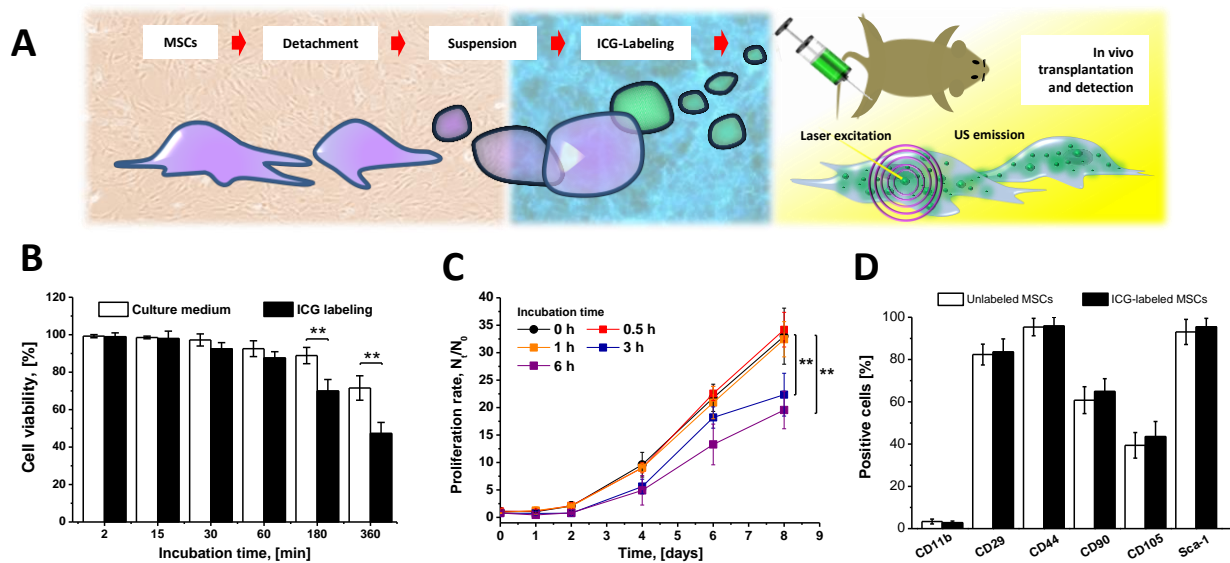
**Author biographies** please see **Supporting  
Information online.**

## References

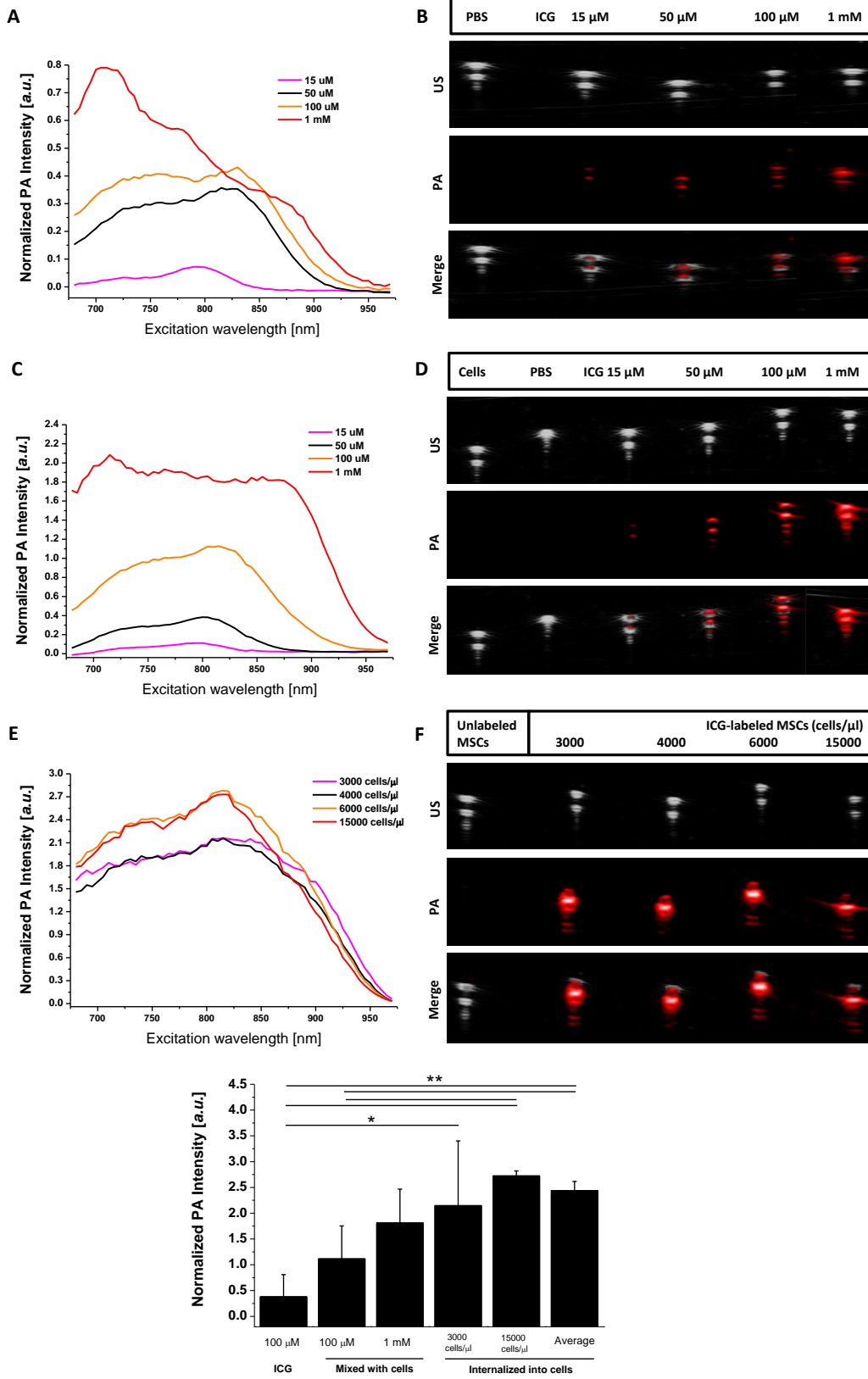
1. E. Buzhor, L. Leshansky, J. Blumenthal, H. Barash, D. Warshawsky, Y. Mazor, and R. Shtrichman, *Regen Med* **9**, 649-672 (2014).
2. X. Wei, X. Yang, Z. P. Han, F. F. Qu, L. Shao, and Y. F. Shi, *Acta Pharmacol Sin* **34**, 747-754 (2013).
3. M. Das, I. B. Sundell, and P. S. Koka, *J Stem Cells* **8**, 1-16 (2013).
4. C. A. Herberts, M. S. Kwa, and H. P. Hermsen, *J Transl Med* **9**, 29 (2011).
5. A. K. Srivastava and J. W. Bulte, *Stem Cell Rev* **10**, 127-144 (2014).
6. M. E. Kupfer and B. M. Ogle, *Biotechnol J* **10**, 1515-1528 (2015).
7. Y. Zhao, A. J. Bower, B. W. Graf, M. D. Boppart, and S. A. Boppart, *Methods Mol Biol* **1052**, 57-76 (2013).
8. E. J. Sutton, T. D. Henning, B. J. Pichler, C. Bremer, and H. E. Daldrup-Link, *Eur Radiol* **18**, 2021-2032 (2008).
9. Z. Yang, Q. Zeng, Z. Ma, Y. Wang, and X. Xu, *J Vis Exp* **31**, 10.3791/1388 (2009).
10. J. E. Kim, S. Kalimuthu, and B. C. Ahn, *Nucl Med Mol Imaging* **49**, 3-10 (2015).
11. Y. Hakamata, T. Murakami, and E. Kobayashi, *Transplantation* **81**, 1179-1184 (2006).
12. R. Bouchard, O. Sahin, and S. S. Emelianov, *IEEE Trans Ultrason Ferroelectr Freq Control* **61**, 450-466 (2014).
13. J. Kim, D. Lee, U. Jung, and C. Kim, *Ultrasonography* **34**, 88-97 (2015).
14. L. Cunha, I. Horvath, S. Ferreira, J. Lemos, P. Costa, D. Vieira, D. S. Veres, K. Szigeti, T. Summavielle, D. Máthé, and L. F. Metello, *Mol Diagn Ther* **18**, 153-173 (2014).
15. X. Yang, E. W. Stein, S. Ashkenazi, and L. V. Wang, *Wiley Interdiscip Rev Nanomed Nanobiotechnol* **1**, 360-368 (2009).
16. S. Manohar, C. Ungureanu, and T. G. Van Leeuwen, *Contrast Media Mol Imaging* **6**, 389-400 (2011).

- 1  
2  
3  
4  
5  
6  
7  
8  
9  
10  
11  
12  
13  
14  
15  
16  
17  
18  
19  
20  
21  
22  
23  
24  
25  
26  
27  
28  
29  
30  
31  
32  
33  
34  
35  
36  
37  
38  
39  
40  
41  
42  
43  
44  
45  
46  
47  
48  
49  
50  
51  
52  
53  
54  
55  
56  
57  
58  
59  
60  
61  
62  
63  
64  
65
17. S. Y. Nam, L. M. Ricles, L. J. Suggs, and S. Y. Emelianov, *PLoS One* **7(5):e37267**, 10.1371/journal.pone.0037267 (2012).
  18. H. Gong, R. Peng, and Z. Liu **65**, 1951-1963 (2013).
  19. A. J. Andersen, P. P. Wibroe, and S. M. Moghimi, *Adv Drug Deliv Rev* **64**, 1700-1705 (2012).
  20. Z. Krpetić, S. Anguissola, D. Garry, P. M. Kelly, and K. A. Dawson, *Adv Exp Med Biol* **811**, 135-156 (2014).
  21. S. Zackrisson, S. M. Van de Ven, and S. S. Gambhir, *Cancer Res* **74**, 979-1004 (2014).
  22. T. Desmettre, J. M. Devoisselle, and S. Mordon, *Surv Ophthalmol* **45**, 15-27 (2000).
  23. B. Yuan, N. Chen, and Q. Zhu, *J Biomed Opt* **9**, 497-503 (2004).
  24. J. T. Alander, I. Kaartinen, A. Laakso, T. Pätälä, T. Spillmann, V. V. Tuchin, M. Venermo, and P. Välisuo, *Int J Biomed Imaging* **2012:940585**, 10.1155/2012/940585 (2012).
  25. H. Abe, T. Mori, T. Umeda, M. Tanaka, Y. Kawai, T. Shimizu, H. Cho, Y. Kubota, Y. Kurumi, and T. Tani, *Surg Today* **41**, 197-202 (2011).
  26. C. Jonak, H. Skvara, R. Kunstfeld, F. Trautinger, and J. A. Schmid, *PLoS One* **6(8):e23972**, 10.1371/journal.pone.0023972 (2011).
  27. R. Alford, H. M. Simpson, J. Duberman, G. C. Hill, M. Ogawa, C. Regino, H. Kobayashi, and P. L. Choyke, *Mol Imaging* **8**, 341-354 (2009).
  28. M. Ogawa, N. Kosaka, P. L. Choyke, and H. Kobayashi, *Cancer Res* **69**, 1268-1272 (2009).
  29. S. E. Boddington, T. D. Henning, P. Jha, C. R. Schlieve, L. Mandrussow, D. DeNardo, H. S. Bernstein, C. Ritner, D. Golovko, Y. Lu, S. Zhao, and H. E. Daldrup-Link, *Cell Transplant* **19**, 55-65 (2010).
  30. V. Sabapathy, J. Mentam, P. M. Jacob, and S. Kumar, *Stem Cells Int* **10.1155:2015**, 10.1155/2015/606415 (2015).
  31. J. D. Ho, R. J. Tsai, S. N. Chen, and H. C. Chen, *Br J Ophthalmol* **88**, 556-559 (2004).
  32. S. Park, J. Kim, M. Jeon, J. Song, and C. Kim, *Sensors (Basel)* **14**, 19660-19668 (2014).
  33. G. Ferrauto, F. Carniato, E. Di Gregorio, L. Tei, M. Botta, and S. Aime, *Nanoscale* **9**, 99-103 (2017).
  34. S. Uthaman, J. S. Bom, H. S. Kim, J. V. John, H. S. Bom, S. J. Kim, J. J. Min, I. Kim, and I. K. Park, *J Biomed Mater Res B Appl Biomater* **104**, 825-34 (2016).
  35. J. C. Kraft and R. J. Y. Ho, *Biochemistry* **53**, 1275-1283 (2014).
  36. E. Portnoy, N. Vakruk, A. Bishara, M. Shmuel, S. Magdassi, J. Golenser, and S. Eyal, *Theranostics* **6**, 167-76 (2016).
  37. K. Serigano, D. Sakai, A. Hiyama, F. Tamura, M. Tanaka, and J. Mochida, *J Orthop Res* **28**, 1267-1275 (2010).
  38. K. Mareschi, D. Rustichelli, R. Calabrese, M. Gunetti, F. Sanavio, S. Castiglia, A. Risso, I. Ferrero, C. Tarella, and F. Fagioli, *Stem Cells Int* **2012:920581**, 10.1155/2012/920581 (2012).
  39. E. Bull, S. Y. Madani, R. Sheth, A. Seifalian, M. Green, and A. M. Seifalian, *Int J Nanomedicine* **9**, 1641-1653 (2014).
  40. J. V. Frangioni and R. J. Hajjar, *Circulation* **110**, 3378-3383 (2004).
-

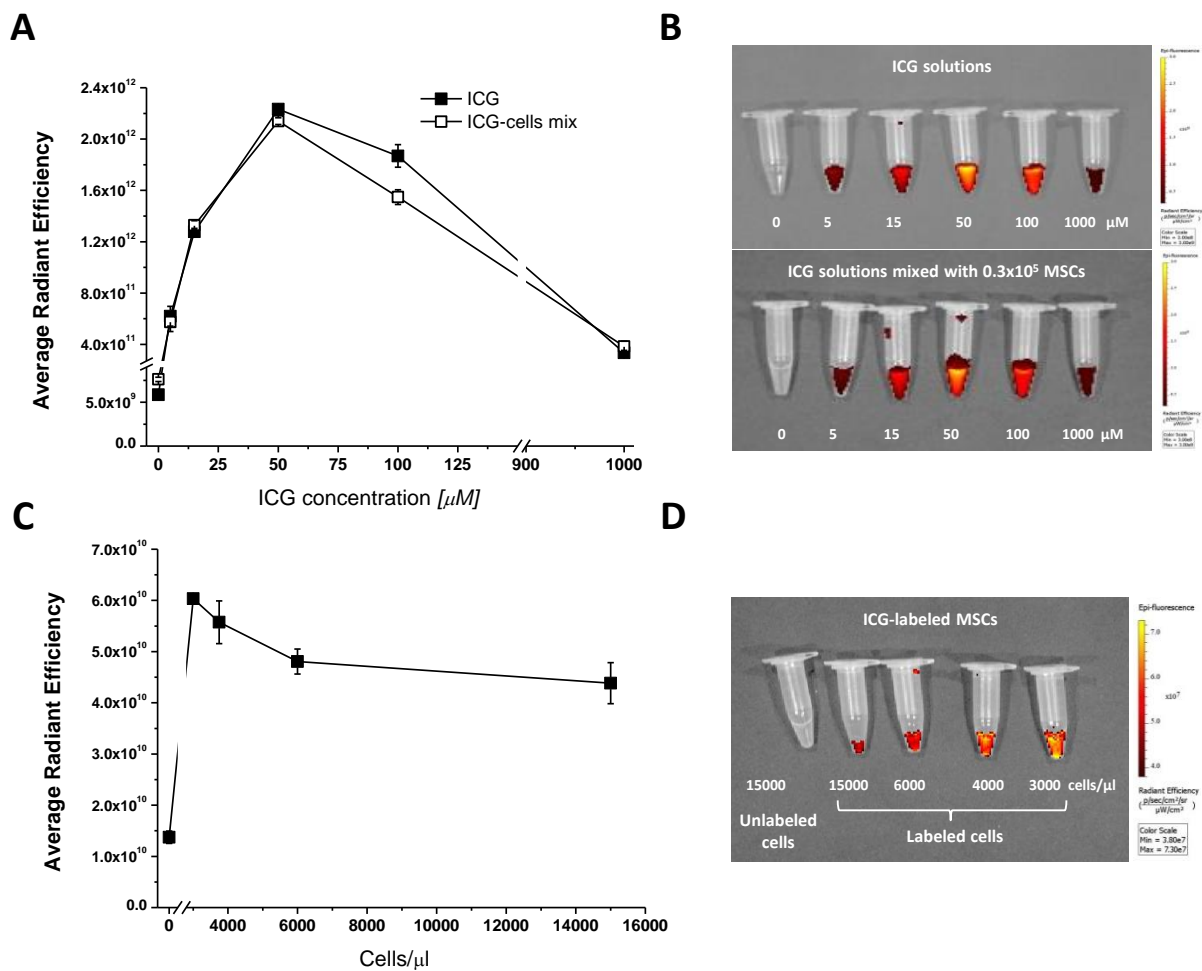
## Figures



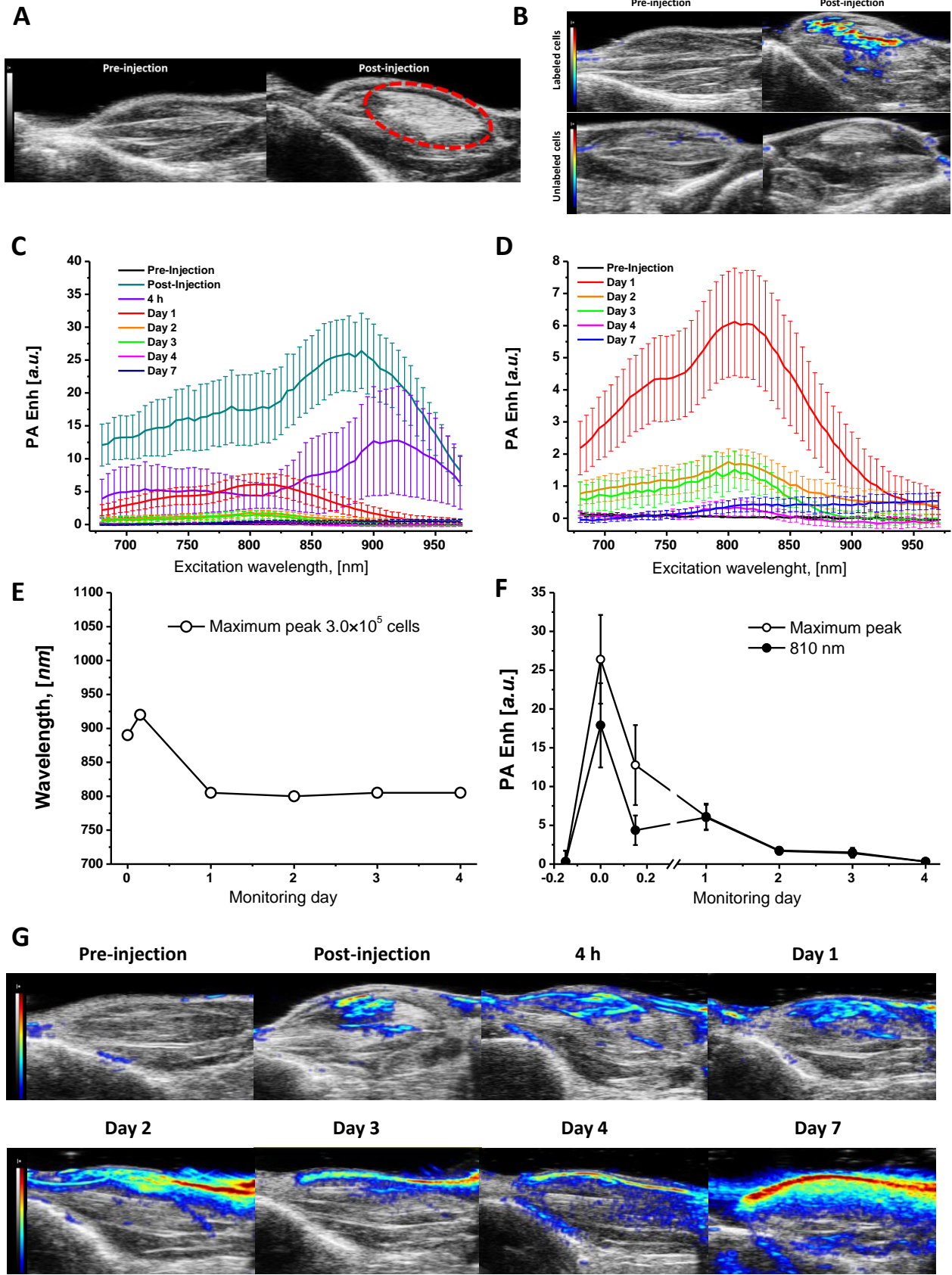
**Figure 1. Cytotoxic effects induced by the ICG.** (A) Schematic diagram of the adopted procedure for ICG-labeling and *in vivo* detection of MSCs. (B) Cell viability estimated on MSCs incubated with 0.25 mg/ml ICG-containing medium for different time ranges. Cells incubated with culture medium were used as control. (C) Proliferation rate of MSCs subjected to the ICG-labeling for different time ranges (0 h refers to control cells that did not undergo the labeling procedure). (D) Marker expression profiles analysed by flow cytometry showing a high conformity between ICG-labeled and unlabeled MSCs. A basic characterization of the primary murine stem cells was provided through the analysis of different surface markers defining the MSC profile ( $CD44^+$ ,  $CD90^+$ ,  $CD29^+$ ,  $CD105^+$ ,  $Sca-1^+$ , and  $CD11b^-$ ).



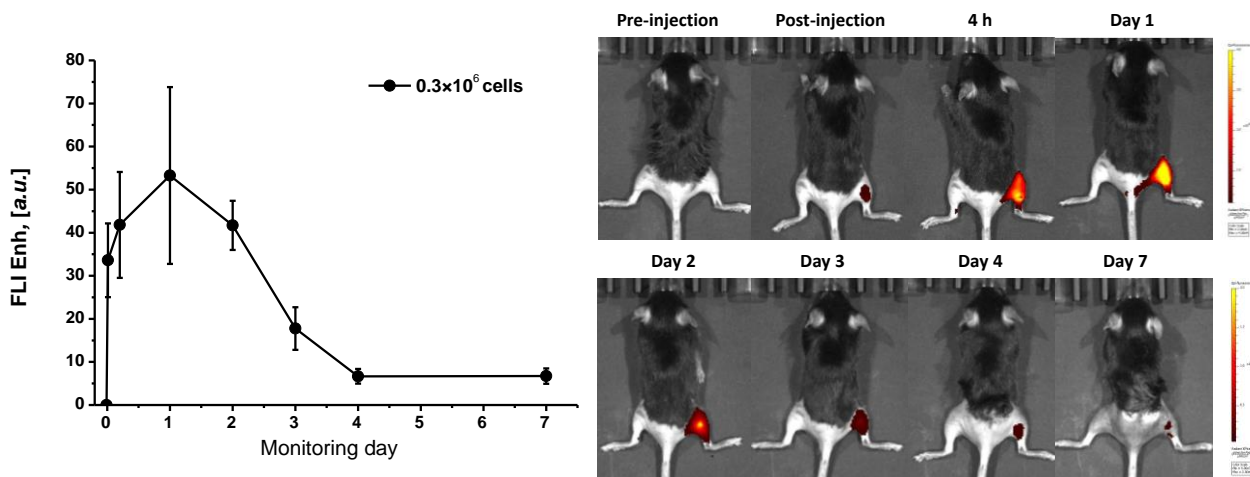
**Figure 2. In vitro PA imaging of ICG.** Photoacoustic spectra (A, C, and E) and representative imaging (B, D, and F) in pure photoacoustic mode (PA), ultrasounds (US) or merged imaging of: aqueous ICG solutions at different concentrations (A and B),  $3.0 \times 10^5$  unlabeled MSCs resuspended in differently concentrated ICG solutions (C and D) and  $3.0 \times 10^5$  ICG-labeled MSCs resuspended at different cell concentrations in PBS (E and F). (G) PA signal quantification at fixed wavelength (810 nm) of ICG in free form, in the presence of cells, and internalized into cells after labeling. ‘Average’ refers to average value of signal from all cell densities conditions. Statistical significance was determined by the unpaired Student *t*-test.



**Figure 3. In vitro optical imaging of ICG.** Fluorescence intensity (as expressed in average radiant efficiency) and representative imaging of aqueous ICG solutions at different concentrations either in the absence or in the presence of  $3.0 \times 10^5$  unlabeled MSCs (A and B), and differently concentrated suspensions of ICG-labeled MSCs (C and D).

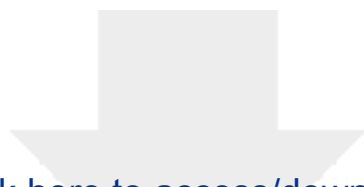


**Figure 4. *In vivo* local PA Signal Intensity after cell transplantation.** (A) Representative B-Mode Ultrasound imaging showing the deposition site of  $3.0 \times 10^5$  unlabeled MSCs after intramuscular transplantation. (B) Representative combined Ultrasound and Photoacoustic (US/PA) images recorded at the PA excitation wavelength of 810 nm, showing the inoculation site before and after the transplantation of  $3.0 \times 10^5$  ICG-labeled MSCs (right hindlimb, top), or an equivalent number of control unlabeled cells (left hindlimb, bottom). (C) Photoacoustic spectra recorded in the inoculation site at variable time ranges after cell deposition, expressed as Photoacoustic enhancement (PA Enh) over the control unlabelled cells. (D) Shape of the photoacoustic spectra recorded at time points starting from day 1. (E) Excitation wavelength of the main peak in the PA spectra during monitoring. (F) Photoacoustic contrast enhancement measured at the excitation wavelength of 810 nm and at that corresponding to the maximum spectral peak. (G) Representative PA monitoring (fixed excitation wavelength: 810 nm) of the cell engraftment over days. ROIs were drawn on the muscular region (internal area of the hindlimb), excluding the unspecific signal generated by the skin-induced reflection artefacts (tissue depth  $\leq 1$  mm).



**Figure 5. *In vivo* optical imaging.** Fluorescence signal intensity measured after the transplantation of  $3.0 \times 10^5$  ICG-labeled MSCs (excitation and emission wavelengths: 745 and 840 nm, respectively) and expressed as Fluorescence Imaging Enhancement (FLI Enh) over the control unlabeled cells (A). Representative optical images showing the time persistence of the fluorescent signal after the cell transplantation (color scale:  $2.0 \times 10^8$ - $4.0 \times 10^9$  for images in the top row,  $4.0 \times 10^7$ - $2.0 \times 10^9$  for images in the bottom row) (B). Calibration bars are shown.

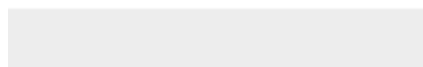
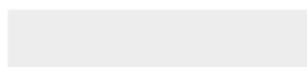




[Click here to access/download](#)

**Supporting Information**

Graphical Abstract for Table of Contents.docx



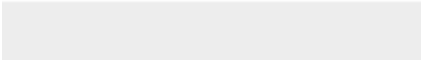



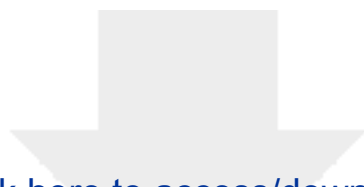
Click here to access/download  
**Supporting Information**  
Supplementary info\_ICGlabeling.docx





Click here to access/download  
**Supporting Information**  
Movies.zip





Click here to access/download  
**Supporting Information**  
CV and photo of authors.docx

